PHILOSOPHICAL TRANSACTIONS OF THE ROYAL SOCIETY A MATHEMATICAL, PHYSICAL & ENGINEERING SCIENCES

Interfacially driven mass transport in joining and coating technologies

The Royal Society

Phil. Trans. R. Soc. Lond. A 1998 **356**, 927-940
doi: 10.1098/rsta.1998.0197

The Royal Society

Interfacially driven mass transport in joining and coating technologies

By David L. Olson and Glen R. Edwards

Center for Welding, Joining and Coating Research, Colorado School of Mines, Golden, CO 80401-1887, USA

The effects of interfacially driven or affected mass transport on (i) hot cracking of alloy weld metal, (ii) the role of interfacial chemical reactions at the leading edge of spreading braze material and (iii) the influence of interfacial tension gradients on abnormal grain growth in thin films are addressed. Hot cracking behaviour will be correlated to interfacial tension gradients in the interdendritic regions of the weld metal. Specific chemical reactions at the interface of the liquid metal braze on a ceramic substrate have been proposed to alter the interfacial force balances causing spreading phenomena. The potential role of interfacial tension gradients on abnormal grain growth in evolution of thin-film microstructures will be discussed.

The influence of Marangoni weld pool stirring and its effect on weld bead morphology has been thoroughly addressed in the literature. This paper will explore other areas in material processing where interfacially driven or affected mass transport can have an effect. First, we will discuss compositional and thermal gradient effects on hot cracking of alloy weld metal. The second area to be discussed will be the role of an interfacial tension gradient at the leading edge of spreading braze material during reaction brazing. The final area to be presented will be the influence of interfacial gradients on abnormal grain growth in thin films.

Keywords: solidification cracking; hot cracking; interdendritic flow; spreading of braze; thin-film growth; abnormal film growth

1. Influence on hot cracking

Hot cracking in weld deposits occurs due to the presence of low melting liquid films that allow boundaries to separate when thermal and shrinkage stresses develop during solidification and cooling (Borland 1960; Arata *et al.* 1976; Clyne & Davies 1979). Here, Fuerer's (1977) model for hot cracking will be first introduced, then combined with the concept of interfacially driven fluid flow to suggest some new insight into the mechanism of interdendritic cracking proposed by Holt *et al.* (1992).

Fuerer's (1977) hot cracking model makes the following assumptions.

(1) During plane front or cellular solidification, shrinkage will occur which is completely fed by residual liquid ahead of the interface.

(2) During dendritic solidification feeding becomes more difficult.

(3) Hot tearing is considered not possible if the rate of feeding (ROF) is larger or equal to the rate of shrinkage (ROS).

(4) Hot tearing becomes possible if the rate of shrinkage exceeds the maximum possible flow rate of feeding.

ROF is described by the following equation:

$$\mathrm{ROF} = \left(\frac{\partial \ln V}{\partial t}\right)_{\mathrm{feeding}} = \frac{g_{\mathrm{L}}^2 d^2 P_{\mathrm{s}}}{24\pi c^3 \eta L^2}, \tag{1.1}$$

where

$$P_{\mathrm{s}} = P_0 + P_{\mathrm{c}} + P_{\mathrm{m}}; \tag{1.2}$$

P_{s} is the effective feeding pressure, P_0 is the atmospheric pressure, P_{c} is capillary pressure, P_{m} is the metallostatic pressure head, g_{L} is the volume of liquid in the dendrite network, c is the tortuosity factor, η is the viscosity of the liquid phase, L is the size of the mushy zone, d is the secondary dendrite arm spacing, V is volume, and t is time.

ROS is described by the following equation:

$$\mathrm{ROS} = \left(\frac{\partial \ln V}{\partial t}\right)_{\mathrm{shrinkage}} = \frac{(\rho_0 - \rho_{\mathrm{s}} + akC_{\mathrm{L}})\varepsilon g_{\mathrm{L}}^{(2-k)}}{\rho(1-k)m_{\mathrm{L}}c_0}, \tag{1.3}$$

where

$$\rho = \rho_{\mathrm{L}} g_{\mathrm{L}} + \rho_{\mathrm{s}}(1 - g_{\mathrm{L}}); \tag{1.4}$$

ρ is the average density, ρ_{L} is the density of the liquid phase, ρ_0 is the density of liquid at the melting point, ρ_{s} is the density of the solid phase, a is the composition coefficient of liquid density, C_{L} is the composition of the liquid at the solid–liquid interface, C_0 is the alloy composition, ε is the average cooling rate during solidification, k is the equilibrium partitioning coefficient, and m_{L} is the slope of the liquidus line.

Figure 1 shows ROF and ROS for an alloy where the temperature (T) is above the eutectic melting temperature (T_{E}) of this alloy. Hot tears will not form as long as ROF is greater than ROS. It becomes important therefore, to have the intersection of the curves (i.e. T_{i}) at a point below the eutectic melting temperature if cracking is to be avoided.

Fluid flow driven by interfacial tension effects will be incorporated into Fuerer's (1977) hot cracking model (Holt *et al.* 1992; Cross *et al.* 1990). The force (F) acting on a surface–interfacial element as a consequence of a surface tension gradient can be described by the following equation:

$$F = -\frac{\partial U}{\partial x} = \frac{\partial \gamma}{\partial x} = \frac{\partial \gamma}{\partial T}\left(\frac{\partial T}{\partial x}\right) + \frac{\partial \gamma}{\partial C}\left(\frac{\partial C}{\partial x}\right), \tag{1.5}$$

where U is the potential energy which, by definition, is the negative of the Helmholtz free energy. Thus, $\partial U/\partial x$ is the negative of $\partial\gamma/\partial x$. Equation (1.5) shows that there will be a force acting on a surface–interfacial element whenever there is a temperature gradient or concentration gradient along that interface, provided $\partial\gamma/\partial T$ and $\partial\gamma/\partial C \neq 0$.

The fluid flow in the weld pool is driven by a surface tension gradient which is very sensitive to surface-active elements. Surface-active elements can cause reversal in the sign of the temperature dependence of the surface tension, and thus promote reversal of the fluid flow in the weld pool. This concept will be applied to fluid flows along the solid–liquid interface during dendritic solidification.

One of the characteristics of dendritic growth is the existence of a temperature gradient along the dendrite axis, with high temperatures at the dendrite tip (liquidus),

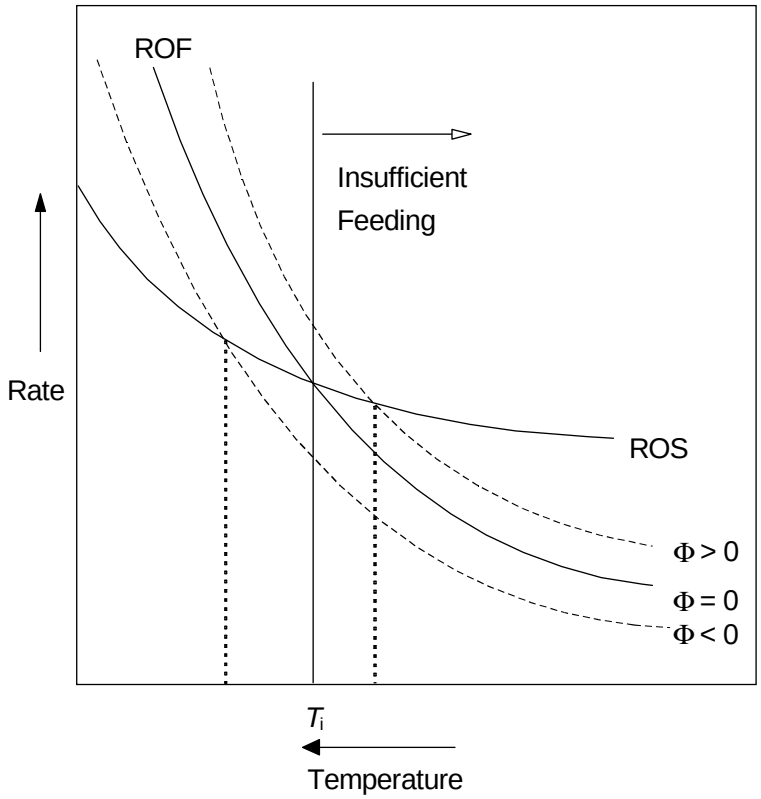

Figure 1. Hypothetical comparison of rate of feeding (ROF) and rate of shrinkage (ROS) as a function of temperature (T) in dendritic solidification; Φ is the pressure resulting from the surface tension gradient (Holt *et al.* 1992).

and low temperatures at the dendrite root (eutectic). This temperature gradient, coupled with $\partial\gamma/\partial T$, will result in a force acting on the interfacial elements along the solid–liquid interface, which will result in a fluid flow along this interface. The direction in which the liquid will flow depends upon the sign of $\partial\gamma/\partial T$.

Cross *et al.* (1990) have combined the Fuerer model with fluid flow driven by interfacial tension. It follows that, apart from the effective feeding pressure P_s, there can also be a 'pressure' resulting from a surface tension gradient acting on the interdendritic fluid (Φ). Equation (1.1) can now be rewritten:

$$\mathrm{ROF} = \frac{g_L^2 d^2 (P_s + \Phi)}{24\pi c^3 \eta L^2}. \tag{1.6}$$

The 'pressure' Φ will, depending on its sign, shift the curve for ROF as shown in figure 1. When, as a consequence of interfacial-tension-driven flow, fluid is forced into the mushy zone, Φ will have a positive value and will result in a lowering of T_i. When, as a consequence of interfacial-tension-driven flow, fluid is forced out of the mushy zone, Φ will have a negative value which will raise T_i, having a deleterious effect on hot cracking resistance. The influence of $\partial\gamma/\partial T$ on interdendritic fluid flow and hot cracking tendency will be shown to be affected by the quantity of surface–interfacial active elements in cases 1 and 2. The influence of solute (i.e. surface–interfacial-active element) redistribution along the dendrite axis will be shown in case 3. The influence

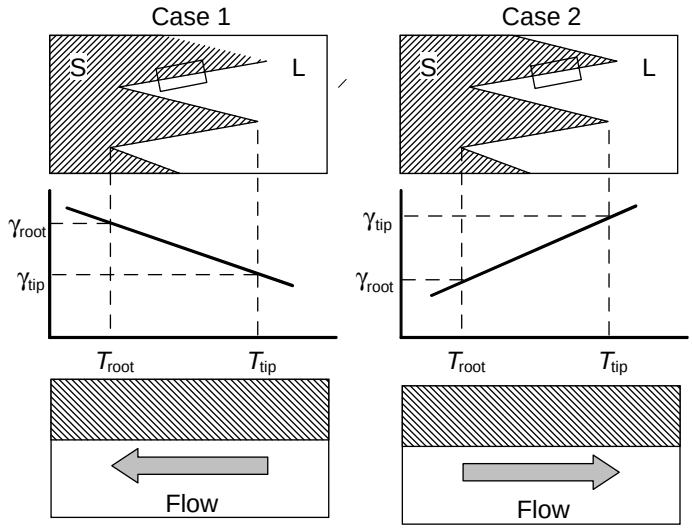

Figure 2. Schematic diagram showing interdendritic fluid flow influenced by the sign of $\mathrm{d}\gamma/\mathrm{d}T$: case 1, $\mathrm{d}\gamma/\mathrm{d}T < 0$ (low sulphur); case 2, $\mathrm{d}\gamma/\mathrm{d}T > 0$ (high sulphur) (Holt *et al.* 1992).

of temperature gradient on interdendritic fluid flow and hot cracking tendency will be shown in cases 4 and 5.

Even though a compositional gradient in a solid surface could not directly create Marangoni flow in an adjacent liquid, the consequence of the solute partitioning during solidification is to create a compositional gradient in the static liquid boundary layer. It is this liquid compositional gradient which causes Marangoni flow within the bulk interdendritic liquid. Such Marangoni flow inhibits the more normal backfilling, thus creating a liquid deficiency and an incipient hot crack.

(*a*) *Influence of impurity concentration*

From equation (1.5), the direction in which the force F works upon an interfacial element can be determined by the sign of $\partial\gamma/\partial T$. In the case of $\partial\gamma/\partial T < 0$ (case 1), fluid will flow from hot areas (γ_{low}) to cooler areas (γ_{high}). In the case of $\partial\gamma/\partial T > 0$ (case 2), fluid will flow from cooler areas (γ_{low}) to hot areas (γ_{high}). Figure 2 shows these two cases. It is seen from this figure that in case 1, fluid is forced into the mushy zone (i.e. $\Phi > 0$), resulting in a lowering of hot-cracking tendency, while in case 2 fluid is forced out of the mushy zone (i.e. $\Phi < 0$), resulting in an increase in hot-cracking tendency.

In practice the sign of $\partial\gamma/\partial T$ depends upon the absence or presence of surface–interfacial active elements. In the case of steels, sulphur has proven to be an important element determining the sign of $\partial\gamma/\partial T$ (Heiple & Roper 1982; Mills & Keene 1990; Burgardt & Campbell 1992). A low sulphur level results in $\partial\gamma/\partial T < 0$ and a high sulphur level results in $\partial\gamma/\partial T > 0$. Consequently, case 1 represents the situation of a low sulphur steel, while case 2 represents the situation of a high sulphur steel. Thus the model predicts a low hot-cracking tendency for low sulphur steels ($\Phi > 0$) and it predicts a high hot-cracking tendency for high sulphur steels ($\Phi < 0$).

During solidification there is also a redistribution of the surface active elements along the dendrite (case 3). This situation can also set up an interfacial tension gradient resulting in an assisted interdendritic fluid flow, as suggested in figure 3.

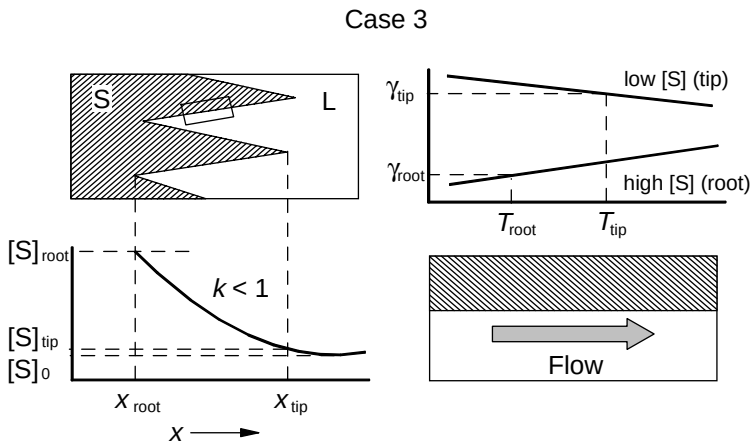

Figure 3. Schematic diagram showing interdendritic sulphur distribution and its influence on fluid flow (case 3) (Holt *et al.* 1992).

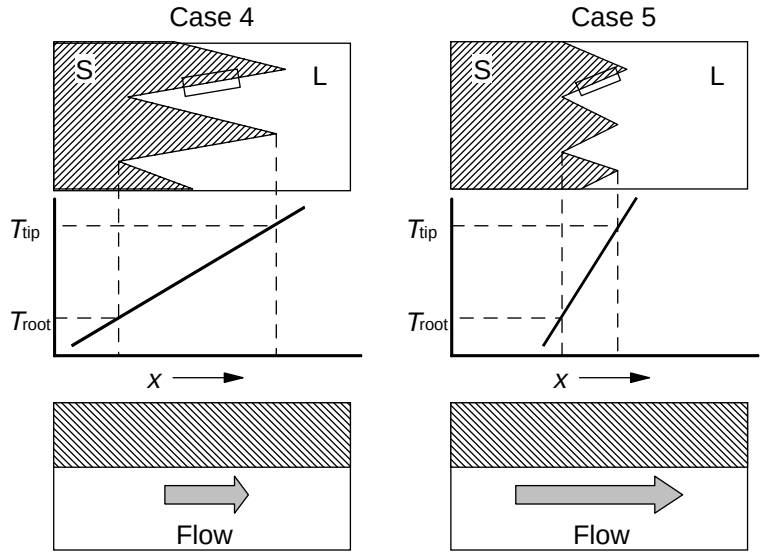

Figure 4. Schematic diagram showing influence of cooling rate on interdendritic fluid flow: case 4, small $\mathrm{d}T/\mathrm{d}x$ (high heat input); case 5, large $\mathrm{d}T/\mathrm{d}x$ (low heat input) (Holt *et al.* 1992).

(*b*) *Influence of temperature gradient*

The influence of the temperature gradient $\partial T/\partial x$ is now addressed. As can be seen from equation (1.5), the value of $\partial T/\partial x$ will influence the force acting on an interfacial element and will therefore influence the interfacial tension-driven fluid flow. In figure 4 this flow is described for a low (case 4) and a high (case 5) value of the temperature gradient and for $\partial\gamma/\partial T > 0$. During welding, a low cooling rate (high heat input) results in a low value of $\partial T/\partial x$, while a high cooling rate (low heat input) results in a high value of $\partial T/\partial x$. Case 4 therefore represents the situation during welding with a low cooling rate, while case 5 represents the situation during welding with a high cooling rate. As can be seen from figure 4, a small temperature gradient results in a relatively weak fluid flow while a large temperature gradient results in a relatively strong fluid flow. In both cases (note $\partial\gamma/\partial T > 0$) fluid is

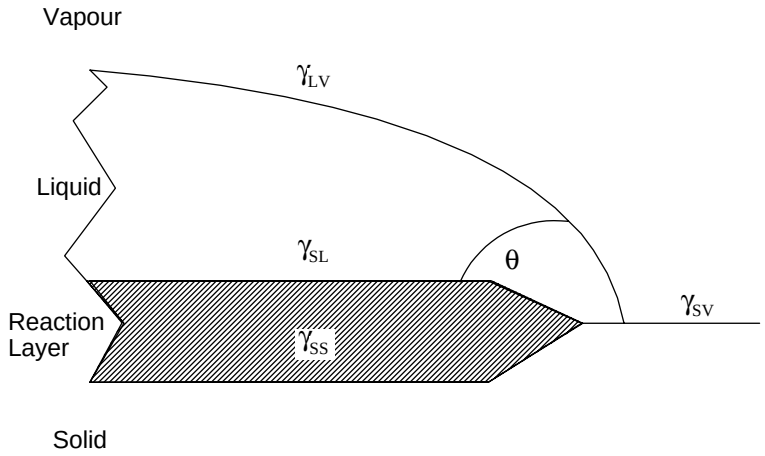

Figure 5. The formation of a reaction product between the reactive liquid brazing material and the solid substrate (Chidambaram *et al.* 1992).

forced out of the mushy zone and therefore $\Phi < 0$. Another factor influenced by the temperature gradient is the size of the mushy zone (L). A small temperature gradient produces a large mushy zone and a large temperature gradient creates a small mushy zone. As can be seen from equation (1.6), both Φ and L influence the rate of feeding (a large mushy zone has a strong detrimental effect on feeding property). Therefore, both factors have to be taken into account before the resulting hot cracking properties can be understood.

The model incorporates the effects of segregation and solute redistribution, which can be used to explain differences in hot-cracking tendencies between stainless steels solidifying as primary ferrite and those alloys solidifying as primary austenite. It also accounts for the effect of differences in cooling rate on hot-cracking susceptibility. It is understood that hot cracking is a complex phenomena involving many different factors in addition to the tendency for backfilling (Cross *et al.* 1990). Which of these factors has overriding influence on cracking susceptibility and the relative importance of interfacial tension in controlling hot crack feeding behaviour has yet to be determined.

2. Influence on spreading

The dynamics of a reactive alloy spreading on a ceramic can be studied as two distinct phenomena: (a) stage I, a reaction layer formation beneath the liquid drop; and (b) stage II, spreading of the liquid ahead of the original triple point.

Stage I. In reactive brazing, the reactive metal attacks the ceramic and forms a reaction product as suggested in figure 5. Chidambaram *et al.* (1992) has demonstrated that a surface thermodynamic criterion could be used to study the wetting and non-wetting metal–ceramic systems. Thermodynamics can only be used to predict wetting and identify the driving force in these systems. Further reaction and spreading of the liquid are entirely kinetic phenomena, and equilibrium thermodynamic will not sufficiently characterize these phenomena. Of interest to this paper is the region at the leading edge of the spreading liquid where the reaction product is not uniformly covering the substrate material, as suggested in figure 6.

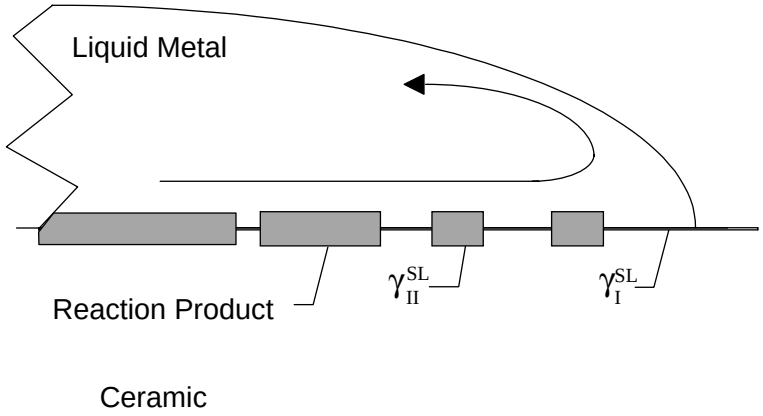

Figure 6. The partly covered reaction product region adjacent to the leading edge of the liquid brazing material. The partly covered reaction product region forms a gradient in liquid–solid interfacial energy and promotes spreading force in the liquid.

Stage II. The movement of the liquid ahead of the original triple point is described as spreading. In non-reactive systems, the driving force for spreading is the decrease in the total surface energy of the system given by the spreading coefficient (Heslot *et al.* 1989):

$$S = \gamma^{SL} - \gamma^{SV} - \gamma^{LV}. \tag{2.1}$$

Spreading occurs when the spreading coefficient is positive. When S is negative, the liquid assumes an equilibrium contact angle. In non-reactive systems, spreading usually occurs after the liquid drop attains a zero degree contact angle. In reactive wetting, this behaviour is not observed; the liquid drop can assume an acute angle even when there is a driving force for spreading. The angle subtended by the drop is a manifestation of various kinetic events, and the angle can decrease only after the liquid drop has moved to an unreacted area.

As mentioned before, spreading in a reactive system is a more complex phenomenon than that described by equation (2.1). When the brazing alloy first comes into contact with the ceramic substrate, no reaction has occurred; hence, the drop does not yet wet the ceramic surface. The interfacial energy, γ_{I}^{SL}, in this situation is largely positive. The alloy then reacts with the ceramic according to stage I kinetics and causes the liquid drop to assume an acute angle, which is the situation where the reaction product has partly covered the surface. The liquid drop experiences two distinct interfacial energies from the reacted and unreacted fractions of the surface. If γ_{II}^{SL} is the interfacial energy between the reaction product and the alloy, the resultant γ^{SL} can be calculated from a rule of mixtures approach:

$$\gamma^{SL} = (1 - X)\gamma_{I}^{SL} + X\gamma_{II}^{SL}, \tag{2.2}$$

where X is the fraction covered at any given instant. This γ^{SL} is a function of coverage on the ceramic surface and, therefore, is a function of time, temperature, and composition of the reactive component of the brazing alloy. Notice that near the leading edge, a gradient in coverage by the reaction product occurs, and thus a gradient in the average interfacial tension is also present.

The observed spreading rate is governed by the balance between the driving force and the resisting force. The viscosity of the alloy would offer resistance to spreading

of the drop. Using the analysis of Lopez *et al.* (1976) for a non-reactive drop, the viscous force is given by

$$F_{\mathrm{v}} = \frac{\mu r^5}{\pi V t}, \tag{2.3}$$

where μ is the viscosity of the molten metal, r is the radius, t is the time and V is the volume of the drop. This term is a function of time and drop radius, but it is not affected by the extent of reaction at the ceramic–metal interface (assuming viscosity is not a function of the reactive metal content in the base alloy).

While the resistance force is the same for a reactive or non-reactive system, the driving force is significantly changed. For a non-reactive spreading system that assumes an instantaneous contact angle ϕ, Yin (1969) calculated the following driving force:

$$F_{\mathrm{s}}\ (\text{non-reactive}) = 2\pi r S_\phi, \tag{2.4}$$

where S_ϕ is the instantaneous spreading coefficient:

$$S_\phi = \gamma^{\mathrm{SL}} - \gamma^{\mathrm{SV}} - \gamma^{\mathrm{LV}} \cos\phi. \tag{2.5}$$

For this situation, the γs are not constants and $\cos\phi$ is determined by requiring the sessile drop to maintain a spherical cap as the drop spreads. In reactive systems, γ^{SL} in the equation for S_ϕ (equation (2.4)) is calculated using the rule of mixtures approach shown in equation (2.2). Therefore, the driving force for reactive spreading is

$$F_{\mathrm{s}}\ (\text{reactive}) = 2\pi r[(1-X)\gamma_{\mathrm{I}}^{\mathrm{SL}} + X\gamma_{\mathrm{II}}^{\mathrm{SL}} - \gamma^{\mathrm{SV}} - \gamma^{\mathrm{LV}}]. \tag{2.6}$$

For a non-reacting system, the resultant force is the difference in driving force and resistive force terms, and a steady-state spreading rate can be calculated (Lopez *et al.* 1976; Yin 1969). In a reactive system, the analysis is complicated by several factors and there is no longer a steady-state solution. Both the driving force and resistive force terms are functions of radius and time while the radius is also a function of time. Therefore, a nonlinear differential equation must be solved to obtain the spreading rate.

The variable which complicates the calculation of the spreading rate is the fraction of surface reacted (X) as a function of time and radius. Estimation of X is further complicated by the depletion of the reactive metal from the liquid metal droplet. As mentioned before, depletion occurs by both the formation of an oxide layer on the metal droplet at the liquid–vapor interface and by the thickening of the reaction layer at the substrate–liquid interface. Now considering the localized gradient in the interfacial tension near the leading edge, there is a second contributing term to the total driving force, F_{TS}:

$$F_{\mathrm{TS}}\ (\text{reactive}) = 2\pi r[(1-X)\gamma_{\mathrm{I}}^{\mathrm{SL}} + X\gamma_{\mathrm{II}}^{\mathrm{SL}} - \gamma^{\mathrm{SV}} - \gamma^{\mathrm{LV}}] + \pi r^2(\gamma_{\mathrm{II}}^{\mathrm{SL}} - \gamma_{\mathrm{I}}^{\mathrm{SL}})\frac{\partial X}{\partial r}, \tag{2.7}$$

where the coverage, X, is a function of r. It is this second term which promotes the continual spreading of the liquid braze material on a ceramic substrate.

A complete understanding of a brazing system culminates in characterization of spreading (stage II). The theory presented further suggests that necessary information for the complete analysis includes the rate of coverage, the rate of interfacial phase formation (stage I kinetics), and the nature of the partial coverage of the reaction product in the region of the leading edge.

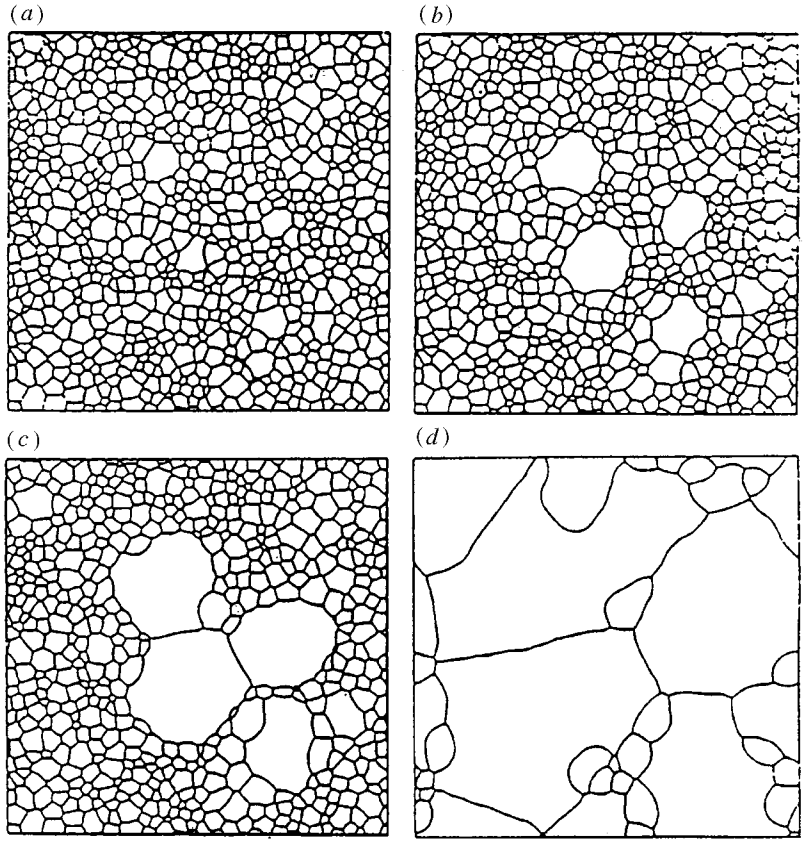

Figure 7. Evolution of the thin-film columnar structure progresses from the stagnation condition (a) to abnormal growth of a few grains (b), (c), to a final large grain structure (d) (Frost 1994).

3. Influence on growth of thin films

The evolution of thin-film microstructures progresses through a series of steps starting with nucleation, then growth to impingement, normal growth, and finally abnormal growth. Depending on the temperature of the substrate and the energy of the arriving atoms, various initial structural configurations will occur and with localized mass transport the structural defects are reduced and the grain growth will go from columnar to a larger equiaxed structure. The resulting thin-film structures were classified by Movchan & Demchishin (1960) and reclassified by Thornton (1988) as zones 1A, 1B, 2, T, and 3. This paper will consider interfacial tension gradients in the thin-film structures as a factor which promotes abnormal growth when the thin-film grains progress from a zone 2 to a zone 3 morphology.

After the grains have nucleated on the substrate and grown to impingement, grain boundary migration results in grains becoming large relative to the film thickness. The resulting grain boundaries become approximately perpendicular to the plane of the film and have a monomodal grain size distribution, as suggested in figure 7a. This arrangement of grain boundaries allows for two-dimensional grain growth modelling (Frost 1994).

Normal grain growth is modelled with the relationship for the velocity, v, given as

$$v = Mk\gamma_{\mathrm{gb}}, \tag{3.1}$$

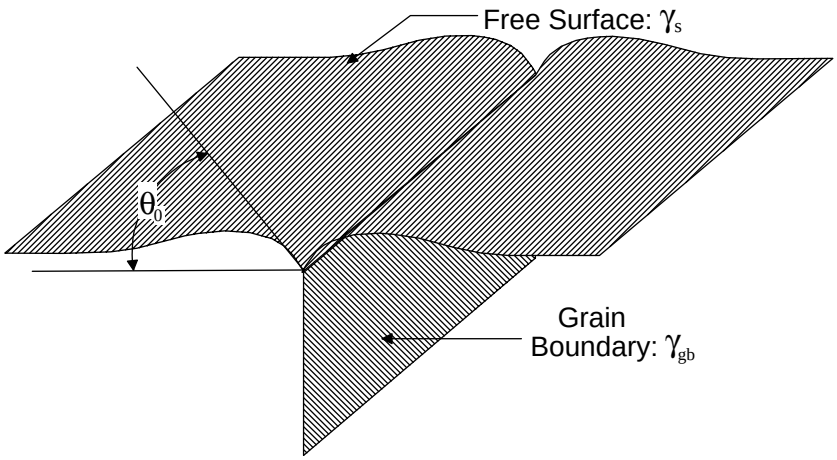

Figure 8. The morphology of a grain boundary groove between two columnar thin-film grains. The grain boundary grooves serve as pinning sites for thin-film grain growth (Mullins 1956).

where k is the curvature, M is the mobility and γ_{gb} is the grain boundary energy. It has been observed that normal grain growth often stagnates when the average grain diameter is two or three times the film thickness (Palmer *et al.* 1989; Frost *et al.* 1958). At the point of stagnation the grains are columnar and their boundaries completely traverse the thickness of the film (Frost 1994).

Mullins (1956) and Dunn (1966) has suggested that the stagnation of normal grain growth in the film is due to grain boundary grooving at the triple points where the grain boundary meets the free surface of the film, as illustrated in figure 8. In his model, surface diffusion redistributes the matter at the triple line so as to achieve equilibrium of the interfacial tensions. The angle at the bottom of the groove is determined by the force balance of the interfacial tensions. This angle is a measure of the force required to allow a grain boundary to escape from the groove. If the force is sufficient to pull the grain boundary to the angle Θ_0, the boundary will climb out of the groove.

If the grain growth proceeds beyond the stagnation of monomodal grain size distribution, abnormal growth occurs where a few grains are released to continue the grain growth (Mullins 1956; Thompson 1985; Thompson & Smith 1984; Wong *et al.* 1986). Figure 7 illustrates this abnormal growth behaviour. If the driving force is sufficient to pull the grain boundary to the angle Θ_c, the grain boundary can climb out of the groove. The force to promote escape or release of the grain boundaries may be the result of in-plane curvature which can pull the grain boundary to a position at which the intersection with the surface deviates from the perpendicular by

$$\Theta_c = \tfrac{1}{2} h k_{crit}, \tag{3.2}$$

where h is the film thickness and the critical curvature for escape is k_{crit}, which is given by

$$k_{crit} = \frac{2\Theta_c}{h} \cong \frac{\gamma_{gb}}{\gamma_s h}. \tag{3.3}$$

Now consider that the thin film has grain boundaries with solute or contaminant compositional gradients which will alter the force balance suggested by Mullins (1956) in figure 9. The compositional gradients suggest an additional force term resulting

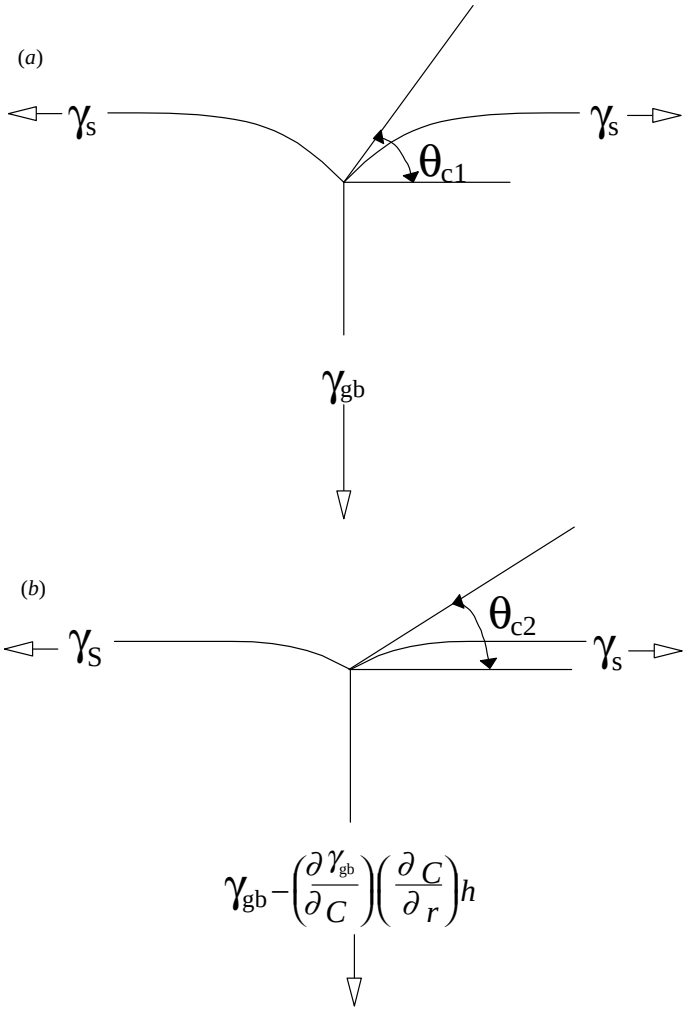

Figure 9. The reduction of the grain boundary tension due to extra force/length resulting from a compositional gradient along the grain boundary, which can be seen by comparing (*a*) with (*b*), to reduce the angle θ_c, which is a direct representation of the pinning force restraining grain growth.

in the following equation:

$$2\gamma_s \cos \Theta_c = \gamma_{gb} - \left(\frac{\partial \gamma_{gb}}{\partial C}\right)\left(\frac{\partial C}{\partial r}\right) h. \tag{3.4}$$

If the grain boundary tension, γ_{gb}, is a function of solute or contaminant composition, then the critical angle to overgrow the grain boundary could be less. This situation would make abnormal growth easier to achieve, and would promote fewer but larger thin-film grains. According to Frost & Thompson (1988), Rolett *et al.* (1985) and Hillert (1965), once the grain boundary is released, two-dimensional growth models based on interfacial forces adequately describe the abnormal growth rate. The actual situation is more complex than presented, since there are two grain boundary grooves, as suggested in figure 10 (one grain boundary groove is on the free surface and the other groove is with the substrate).

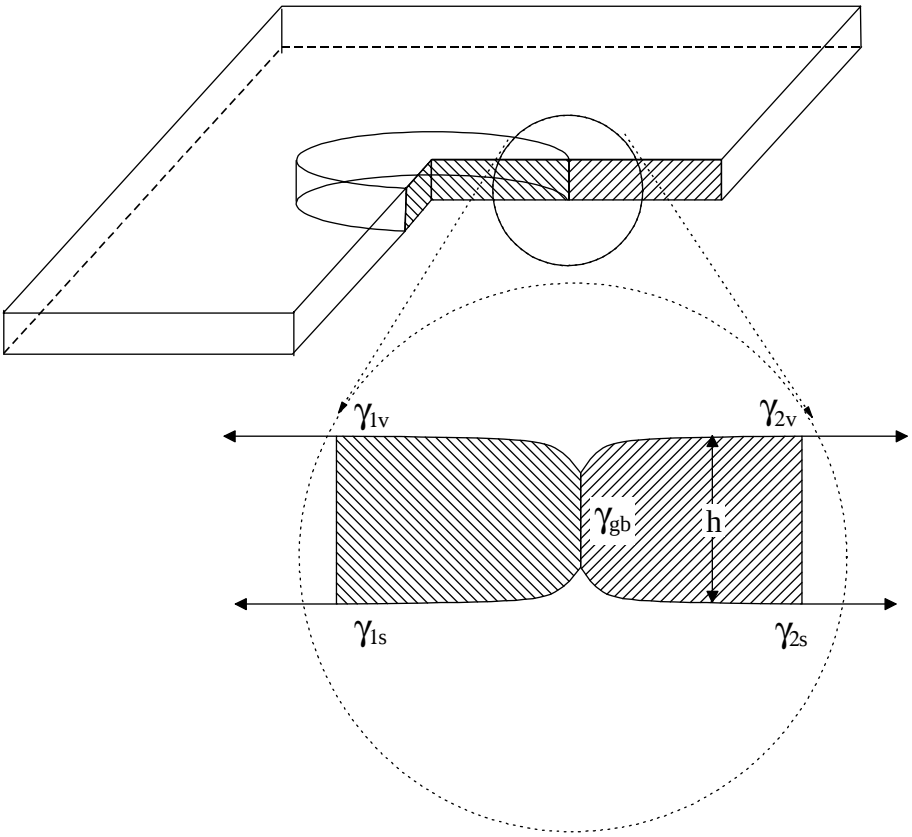

Figure 10. A difference in interfacial energies for the cylindrical grain and the neighbouring grain results in a driving force for grain growth after the grain boundary has been released (Frost 1994).

A suggested driving force for abnormal grain growth is the difference in surface energies for two neighbouring grains, $\Delta\gamma = \gamma_1 - \gamma_2$. The effect of this difference on the grain boundary migration rate is a function of the thin-film thickness, h. This concept is suggested in figure 10 (Frost 1994), where a circular grain in a thin film is shown experiencing the driving forces due to grain boundary capillarity.

By considering the driving force due to both the difference in the specific free surface energies between the inside and outside of the cylindrical boundary and the grain boundary capillarity, the total migration velocity, v, can be described by

$$v = v_{\mathrm{gb}} + v_{\mathrm{s}}, \tag{3.5}$$

where

$$v_{\mathrm{gb}} = M\gamma_{\mathrm{gb}}k \tag{3.6}$$

and

$$v_{\mathrm{s}} = M\frac{2\Delta\gamma}{h}. \tag{3.7}$$

The $\Delta\gamma$ is assumed to be the result of the difference in surface energy due to crystal orientation between neighbouring grains. This situation is not very likely to be the primary factor since the thin-film columnar grains are growing in a preferred direction and thus exposing approximately the same crystal surface. A more likely

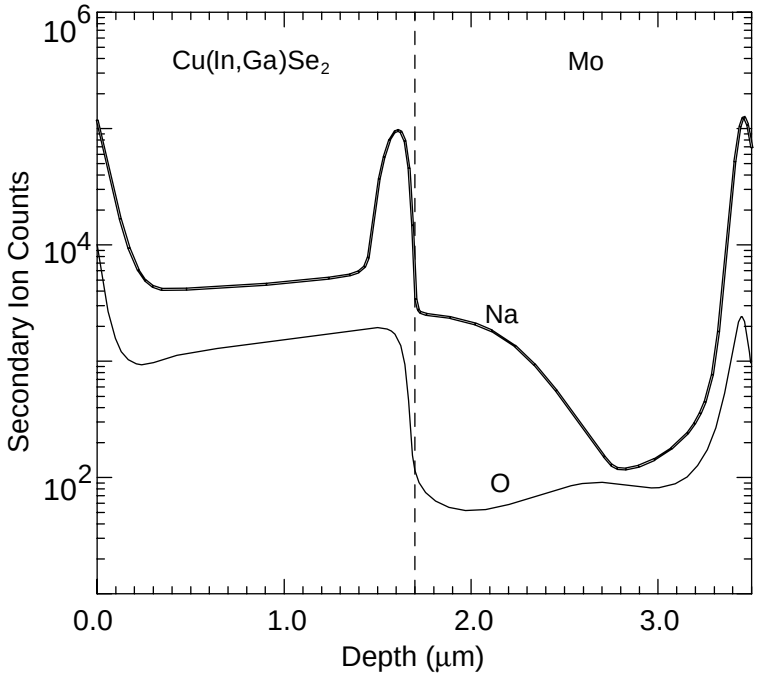

Figure 11. The compositional profile for sodium and oxygen content, surface active contaminants, across a $Cu(In,Ga)Se_2$–molybdenum thin film deposited on a soda glass. Notice the localized compositional gradients (after Scofield *et al.* 1994).

situation is a variation in surface contamination across the thin-film surface, grain to grain.

It is common to find compositional gradients in compound thin films, and these compositional gradients would be expected to alter the interfacial forces and thus the growth behaviour (Probst *et al.* 1996; Scofield *et al.* 1994; Kim & Thompson 1990). The influence of compositional gradients of sodium in copper–indium–gallium diselinide depositions have been shown to promote thin-film grain growth (Probst *et al.* 1996; Scofield *et al.* 1994). The source of the sodium is the soda glass substrate. This compositional gradient across a CIS–molybdenum deposit on a soda glass substrate can be seen in figure 11. Kim & Thompson (1990) have also reported the effect of dopants on surface-energy-driven secondary grain growth in silicon films.

4. Conclusion

The joining and coating processes produce material with significant gradients in composition, microstructure and properties. These gradients must be considered in achieving a mechanistic understanding of the microstructural evolution and the microstructure-property relationships of these processed materials.

The authors appreciate and acknowledge the research support of the Office of Naval Research.

References

Arata, Y., Matsuda, F., Nakata, K. & Sasaki, I. 1976 *Trans. JWRI* **5**, 53.
Borland, J. C. 1960 *Br. Welding J.* **7**, 508.

Burgardt, P. & Campbell, R. D. 1992 *Key Engng Mater.* **69/70**, 379–416.

Chidambaram, P. R., Edwards G. R. & Olson, D. L. 1992 *Met. Trans.* B **23**, 215.

Clyne, T. W. & Davies, G. J. 1979 *TMS Proc. Int. Conf. Solidification, Sheffield, UK*, p. 275.

Cross, C. E., Tack, W. T. & Loechel, J. L. W. 1990 *ASM Conf. Proc. On Weldability of Materials, Detroit*, p. 275.

Dunn, C. G. 1966 *Acta Metall.* **14**, 221–222.

Frost, H. J. 1994 *Mater. Character.* **32**, 257–273.

Frost, H. J. & Thompson, C. V. 1988 *J. Electron. Mater.* **17**, 447–458.

Frost, H. J., Thompson, C. V. & Walton, D. T. 1958 *Acta Metall.* **6**, 414–427.

Fuerer, U. 1977 *Proc. Int. Sym. Eng. Alloys, Delft, The Netherlands*, p. 131.

Heiple, C. R. & Roper, J. R. 1982 *Welding J.* **61**, 97.

Heslot, F., Fraysse, N. & Cazabat, A. M. 1989 *Nature* **338**, 640.

Hillert, M. 1965 *Acta Metall.* **13**, 227–238.

Holt, M., Cross, C. E. & Olson, D. L. 1992 *Scripta Metall. Mater.* **26**, 1119–1124.

Kim, H. J. & Thompson, C. V. 1990 *J. Appl. Phys.* **67**, 757–767.

Lopez, J., Miller, C. A. & Ruckenstein, E. 1976 *J. Colloid. Interf. Sci.* **56**, 460.

Mills, K. C. & Keene, B. J. 1990 *Int. Mater. Rev.* **35**, 185.

Movchan, B. A. & Demchishin, A. V. 1969 *Fiz. Met. Metall.* **28**, 653.

Mullins, W. W. 1956 *J. Appl. Phys.* **27**, 900–904.

Palmer, J. E., Thompson, C. V. & Smith, H. I. 1987 *J. Appl. Phys.* **62**, 2492.

Probst, V., Krag, F., Rimmasch, J., Riedl, W., Stetter, W., Harms, H. & Eibl, O. 1996 *Mat. Res. Soc. Symp. Proc. on Thin Films for Photovoltaics and Related Device Application*, vol. 426, p. 165.

Rollett, A. D., Srolovitz, D. J. & Anderson, M. P. 1985 *Acta. Metall.* **33**, 2233–2247.

Scofield, J. H., Asher, S., Albin, D., Tuttle, J., Contreas, M., Niles, D., Reedy, R., Tenant, A. & Noufi, R. 1994 *Proc. 1st WCPEC, 5–9/12/94, Honolulu, Hawaii*, pp. 1647–1667. IEEE.

Thornton, J. A. 1988 *A. Rev. Mater. Sci.* **7**, 239.

Thompson, C. V. 1985 *J. Appl. Phys.* **58**, 763–772.

Thompson, C. V. & Smith, H. I. 1984 *Appl. Phys. Lett.* **44**, 603–605.

Wong, C. C., Smith, H. I. & Thompson, C. V. 1986 *Appl. Phys. Lett.* **48**, 335.

Yin, T. P. 1969 *J. Phys. Chem.* **7**, 2413.

Discussion

R. C. Cochrane (*School of Materials, University of Leeds, UK*). What is the scale at which the abnormal grain growth in thin films would be expected to occur? Is it at a scale of μm or tens of μm? (It could occur up to 0.5 mm or so!)

D. L. Olson. It has been observed that abnormal grain growth initiates when the grain diameter in the plane of the film is 2–3 times the film thickness. Typical thin-film thicknesses are from 2–10 μm.